ACS APPLIED BIO MATERIALS
Cite This: ACS Appl. Bio Mater. 2019, 2, 3562−3572
Article
www.acsabm.org

Modulating Mechanical Properties of Collagen−Lignin Composites

Jorge A. Belgodere,[†] Syed A. Zamin,[†] Ryan M. Kalinoski,[‡] Carlos E. Astete,[†] Joseph C. Penrod,[†] Katie M. Hamel,[†] Bert C. Lynn,[¶] Jai S. Rudra,[§,∥] Jian Shi,*[,¶] and Jangwook P. Jung*[,‡]

[†]Biological and Agricultural Engineering, Louisiana State University, 149 E.B. Doran Hall, Baton Rouge, Louisiana 70803, United States

[‡]Biosystems and Agricultural Engineering, University of Kentucky, 128 C.E. Barnhart Building, Lexington, Kentucky 40546, United States

[¶]Chemistry, University of Kentucky, 125 Chemistry/Physics Building, Lexington, Kentucky 40506, United States

[§]Department of Pharmacology and Toxicology, University of Texas Medical Branch, 301 University Boulevard, Galveston, Texas 77555, United States

Supporting Information

ABSTRACT: Three-dimensional matrices of collagen type I (Col I) are widely used in tissue engineering applications for its abundance in many tissues, bioactivity with many cell types, and excellent biocompatibility. Inspired by the structural role of lignin in a plant tissue, we found that sodium lignosulfonate (SLS) and an alkali-extracted lignin from switchgrass (SG) increased the stiffness of Col I gels. SLS and SG enhanced the stiffness of Col I gels from 52 to 670 Pa and 52 to 320 Pa, respectively, and attenuated shear-thinning properties, with the formulation of 1.8 mg/mL Col I and 5.0 mg/mL SLS or SG. In 2D cultures, the cytotoxicity of collagen−SLS to adipose-derived stromal cells was not observed and the cell viability was maintained over 7 days in 3D cultures. Collagen−SLS composites did not elicit immunogenicity when compared to SLS-only groups. Our collagen−SLS composites present a case that exploits lignins as an enhancer of mechanical properties of Col I without adverse cytotoxicity and immunogenicity for *in vitro* scaffolds or *in vivo* tissue repairs.

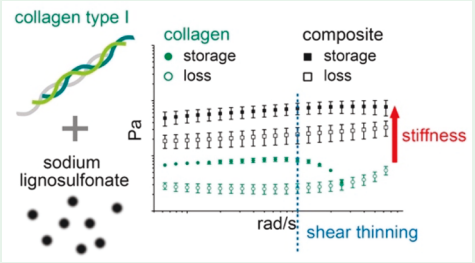

KEYWORDS: *extracellular matrix composite, sodium lignosulfonate, shear-thinning, physical co-assembly, stem cells*

INTRODUCTION

Collagen type I (Col I) has been extensively used for 3D cell culture gels and engineered tissue models.[1−6] Collagen gels are relatively easy to prepare and apply, but they are mechanically weak for scaffolds that need high shear resistance. To enhance mechanical properties of collagen gels, several cross-linking methods were employed with ribose (glycation),[6] methacrylate,[7,8] and glutaraldehyde.[9−11] Non-enzymatic glycation improved the stiffness of collagen around 4-fold (175−730 Pa) while maintaining the native fiber structure without employing any synthetic materials.[6] Conjugation of methacrylamide also improved mechanical stability through photo-cross-linking.[7,8] Collagen methacrylamide (CMA) retains the self-assembly, biodegradability, and natural bioactivity of Col I, while the stiffness is increased from self-assembled collagen (13.5 kPa) to covalently cross-linked collagen (162 kPa). Glutaraldehyde (GTA) cross-linking[11] also significantly increased the stiffness of 4 mg/mL collagen gels from 16 to 137 Pa.[10] Although GTA improves collagen mechanical properties, toxicity could be a concern as depolymerization of GTA cross-links releases GTA into the recipient.[11] Thus, we looked for simple, straightforward approaches to stiffen collagen gels without adverse effect in cells and host tissue, which are beneficial for large tissue formation without introducing additional treatment or cross-linking chemistry. In addition, ease of application with abundant source and structural support would be beneficial to use in collagen-based matrices with multiple extracellular matrix (ECM) proteins for regenerative medicine applications.[12−14] Toward these goals, we physically incorporated lignin in Col I gels to enhance stiffness and to attenuate shear-thinning properties.

Lignin is one of the most abundant naturally occurring polyphenolic organic polymers, ranging between 15 and 30% of cell wall content in typical terrestrial plants.[15,16] Present mainly in the secondary cell wall layers (middle lamella), lignin interacts with hemicellulose and cellulose, thus playing a crucial role for the structural integrity of plant cell walls.[15] The high density of several functional groups (aliphatic, phenolic, carboxylic, carbonyl, and methoxyl groups) make lignin an affordable and attractive molecule for biomedical and other applications for valorization[17−20] (see Figure S1, Supporting Information). From a chemistry perspective, the polyaromatic structure resembles 3,4-dihydroxyphenyal acetic acid, a

Received: May 25, 2019
Accepted: July 30, 2019
Published: July 30, 2019

DOI: 10.1021/acsabm.9b00444
ACS Appl. Bio Mater. 2019, 2, 3562−3572

derivative of 3,4-dihydroxyphenylalanine (DOPA) responsible for the strong adhesion of mussel.[21,22]

Neither lignin or Col I is a new type of biomaterial. However, our inspiration originates from the structural role of lignin in plant cell walls, which could alter mechanical properties of physically assembled collagen scaffolds. Both lignin and Col I are widely available biomaterials, while the specific combination of the two biomaterials and the applicable type of lignin to reinforce the mechanical properties of collagen scaffolds have not been investigated yet to our knowledge. Thus, we hypothesized that lignin incorporation will stiffen self-assembled Col I gels, creating biomaterials suitable for tissue engineering application that requires stable, self-supporting structures. In this study, we investigated viscoelastic properties of collagen−lignin composites using lignins extracted from three representative biomass feedstocks and sodium lignosulfonate (SLS) for the exceptional enhancement of mechanical properties. Cytotoxicity and growth of human adipose-derived stromal cells (ASCs) as well as murine embryonic stem cells (ESCs) were evaluated with the collagen−SLS scaffolds. Immunogenicity of the collagen−SLS composites was also assessed using BALB/c murine models.

MATERIALS AND METHODS

Scheme 1 outlines the overall experimental procedures including chemical characterization, synthesis, and material properties in the current study.

Scheme 1. Overall Experimental Procedures Performed in the Current Study

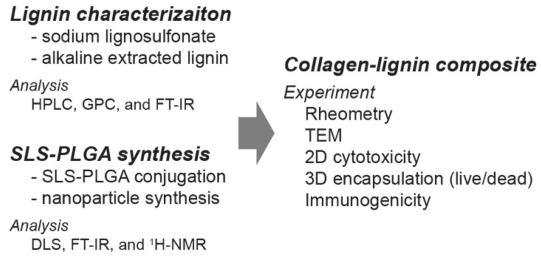

SLS. SLS was obtained and used without any modifications (TCI Chemicals, cat. no. L0098, lot no. V5VJF-IC, >94% purity)

Monolignols. Each monolignol (coniferyl (G), sinapyl (S), and coumaryl (H) alcohol) was synthesized from its corresponding acid, ferulic acid (cat. no. 128708-5G, Sigma-Aldrich), sinapinic acid (cat. no. D7927-1G, Sigma-Aldrich), and coumaric acid (cat. no. C9008-10G, Sigma-Aldrich), respectively. Further details of the synthesis are described in the Supporting Information.

Alkali-Extracted Lignin. Three biomass feedstocks, hybrid poplar, lodge pole pine, and switchgrass, representing distinctive monolignol compositions, were obtained from the Idaho National Laboratory. Before pretreatment, the biomass was ground using a Thomas Model 4 Wiley Mill (Thomas Scientific) to 1 mm particles. The ground biomass was then sieved with a Ro-Tap testing sieve shaker (Model B, W. S. Tyler Industrial Group), which produced a particle size range of 0.25−0.425 mm. For dilute alkaline pretreatment, 2 g (dry weight) of biomass was mixed with 18 mL of NaOH solution (50 mM) in a tubular reactor (made of stainless steel SS316, 6″ in length and 3/4″ in outer diameter). The reactors were then capped, and the premixed slurry was presoaked at room temperature (RT) for 4 h in the reactors. The rector vessels were then transferred to a temperature-controlled sand bath, where pretreatment was conducted at 140 ± 2 °C for 1 h.[23,24] After pretreatment, the liquid fraction was separated using 300 mesh nylon filters and adjusted to a pH of 2.0 with 1 M HCl to precipitate the lignin. The precipitated lignin was then washed 4 times with 40 mL deionized (DI) water for each wash, and the solids were separated from the liquid by centrifugation at 4000*g*. To remove sugar from precipitated lignin, the three alkaline lignin samples were enzymatically hydrolyzed by following the National Renewable Energy Laboratory (NREL) laboratory analytical procedure.[25] The cellulase (CTec2, batch no. VCS00002, Novozymes Inc.) and hemicellulase (HTec2, batch no. VHN00003, Novozymes Inc.) enzymes were premixed at a 9:1 (v/v). The saccharification was performed at 50 °C for 72 h at an enzyme loading of 10 mg enzyme protein/g starting biomass (dry weight) in a 50 mM citrate buffer solution (pH 4.8) on an orbital shaker (Thermo Forma 435, ThermoFisher Scientific). Then, the recovered lignin was washed with warm water and then lyophilized (Freezone Model 77530, Labconco) for 48 h.

High-Performance Liquid Chromatography (HPLC). Structural carbohydrates and the lignin composition of alkaline pretreated poplar, pine, and switchgrass lignins were determined by a two-step acidolysis method according to NREL analytical procedures.[26] The sugar concentration was analyzed by HPLC (Ultimate 3000, Dionex Corporation) equipped with a refractive index detector and using a Bio-Rad Aminex HPX-87H column and guard assembly. The HPLC was run using 5 mM H_2SO_4 as a mobile phase at a flow rate of 0.4 mL/min and a column temperature of 50 °C.

Gel Permeation Chromatography (GPC). Lignin samples were prepared for GPC by the acetylation method.[27] Lignin samples of 10 mg were dissolved in a 92:8 (v/v) anhydrous acetic acid and acetyl bromide solvent mixture for 2 h at 50 °C. Then the excess solvent was dried using nitrogen gas, and the acetylated lignin was dissolved in tetrahydrofuran (THF) and stored at RT before analysis. The weight distribution profile, weight-average molecular weight ($\overline{M}_w$), number-average molecular weight ($\overline{M}_n$), and polydispersity index (PDI) were determined by a HPLC system (Ultimate 3000, Dionex Corporation). The system was equipped with a UV detector and a mixed-D PL gel

Scheme 2. Polymerization Method To Synthesize the SLS−PLGA Copolymer

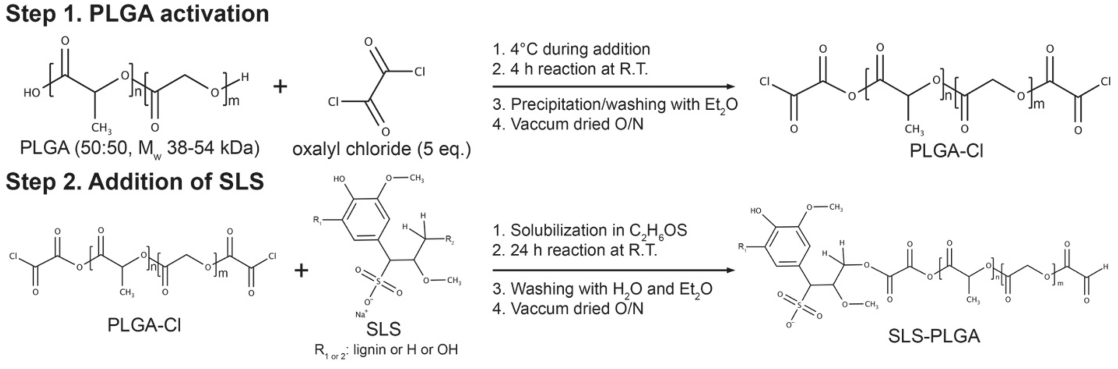

DOI: 10.1021/acsabm.9b00444
ACS Appl. Bio Mater. 2019, 2, 3562−3572

column (5 μm particle size, 300 mm × 7.5 mm, Polymer Laboratories, Amherst, MA). The mobile phase utilized THF at a flow rate of 0.5 mL/min at 80 °C. Column eluting materials were monitored using a UV wavelength of 290 nm, and the chromatography was calibrated using polystyrene standards (cat. no. 48937, Sigma-Aldrich).

Fourier-Transform Infrared (FT-IR) Spectroscopy. Infrared spectra of alkali-extracted lignins and SLS were recorded using a Thermo Nicolet Nexus 870 ESP ATR−FTIR spectrometer. The samples were compressed to 12 psi using a spring-loaded jack that was set onto an attenuated total reflection crystal (ATR). For each time of measurement, an average of 64 scans was recorded between 400 and 4000 cm^{-1} with a resolution of 1.928 cm^{-1}. Using Omnic 6.1a software, the raw FTIR spectra were normalized and baseline corrected in the range 800−2000 cm^{-1}. Infrared spectra of SLS, poly(lactic-*co*-glycolic acid) (PLGA, 50:50, M_W 38 000−54 000 Da, cat. no. 719900−5G, Sigma-Aldrich), and SLS−PLGA, samples were placed in the Pike single-bounce diamond/ZnSe ATR at RT. Using a Brunker Tensor 27 FTIR spectrometer, the absorbance was recorded between 400 and 4000 cm^{-1}.

Synthesis of SLS−PLGA Nanoparticles. The synthesis steps and reaction schemes of SLS-PLA copolymerization are depicted in Scheme 2.

First, the conjugation of SLS with PLGA involved a two-step process based on acylation. Briefly, the first step involved PLGA chlorination, and the reaction was performed in a three neck 500 mL round-bottom flask under mild stirring. Nitrogen gas bubbling and an outlet connected to a wash bottle containing sodium hydroxide solution were used to trap any hydrogen chloride that formed. The dissolution of 2 g of PLGA (50:50) in 30 mL of dichloromethane (DCM, cat. no. 61030-0010, Acros Organics, 99.9%) was performed at RT under mild stirring for 15 min. An excess of oxalyl chloride (5 equiv) (cat. no. AC129610250, Acros Organics, 98%) was slowly added to the PLGA solution. The solution was cooled down to 4 °C during addition. After addition, the reaction was completed at RT for 4 h. Finally, the polymers were precipitated and washed with ethyl ether twice before being vacuum-dried overnight. The second reaction was performed by the addition of SLS. Several ratios between PLGA and SLS were used to study the effect of SLS in the polymeric nanoparticles, and here we have outlined the steps for the 1:2 ratio. The dry SLS (500 mg) was dissolved in 20 mL of dimethyl sulfoxide (DMSO, cat. no. 61042-0010, Acros Organics, 99.7%) at RT under mild mixing. Also, 1 g of PLGA-Cl was dissolved in 20 mL of DMSO, and it was slowly added to the SLS solution. The reaction was performed at RT and stopped after 24 h. SLS−PLGA graft polymers were washed with cold water and ether to remove the unreacted SLS and dried under a high vacuum overnight, and samples were stored at −20 °C for further characterization and nanoparticles synthesis.

The synthesis of SLS−PLGA nanoparticles was followed by an emulsion evaporation technique. Briefly, 40 mg of the biopolymer was dissolved in 1 mL of ethyl acetate at RT for 30 min. The organic phase was dropwise added to 10 mL of water in an ice bath during sonication. The final emulsion was sonicated with a Vibra-Cell VC 750 (Sonics & Materials Inc.) for a total of 12 min (40% amplitude, 5 s "on" and 2 s "off"). Next, the solvent was evaporated in a rotavapor Buchi R300 (Buchi Corporation) under vacuum. Once finished, D-(+)-trehalose (cat. no.182551000, Acros Organics, 99%) was added to protect the nanoparticles during the freeze-drying process. The clear suspension was freeze-dried (Labconco Corp.) for 48 h, and the final powder was stored at −20 °C for further use and characterization. All of the SLS−PLGA nanoparticles synthesized followed the same protocol.

Dynamic Light Scattering (DLS). The size of SLS−PLGA nanoparticles and SLS nanoparticles was measured by DLS using a Malvern Zetasizer Nano ZS (Malvern Panalytical Inc.). The samples were diluted to 0.4 mg/mL with low resistivity water, and 1.2 mL of the sample was placed in a cuvette for measurement. The readings were performed at a pH of 6 and a temperature of 25 °C, and the measurement angle was 173°.

^{1}H Nuclear Magnetic Resonance (^{1}H NMR) Spectroscopy. Samples were prepared in dimethyl sulfoxide (DMSO-d_6 or $(CD_3)_2SO$, cat. no. AA3651748, Alfa Aesar, 99.9%), and ^{1}H NMR spectra were measured by a Brunker AVIII 500 MHz NMR spectrometer (Brunker) at RT. SLS−PLGA ^{1}H NMR (500 MHz, $(CD_3)_2SO$): δ 5.19−5.28 (m, (−O<u>CH</u>(CH_3)CO−), 4.81−4.96 (m, (−O<u>CH_2</u>COO−), 1.47−1.48 (d, (−OCH(<u>CH_3</u>)CO−) ppm. PLGA: δ 5.19−5.28 (m, (−O<u>CH</u>(CH_3)CO−), 4.81−4.96 (m, (−O<u>CH_2</u>COO−), 1.47−1.48 (d, (−OCH(<u>CH_3</u>)CO−) ppm. Water δ 3.33 ppm and $(CD_3)_2SO$ δ 2.51 ppm.

Oscillating Rheometry. Samples for oscillating rheometry were cast using a polydimethylsiloxane (PDMS, 10:1 ratio of the elastomer base and elastomer curing agent, Sylgard 184, Dow Corning) mold of 8 mm in diameter for 1 h at 37 °C. Using a TA Discovery HR-2 rheometer with an 8 mm parallel plate, storage (G') and loss (G'') moduli of composites were determined from 0.628 to 62.8 (rad/s) at a strain of 10% by frequency sweeping.

Transmission Electron Microscopy (TEM). Samples were prepared by diluting the 1.8 mg/mL collagen solutions, with and without 5.0 mg/mL SLS, with deionized ultrafiltered water (DIUF, cat. no. W2-20, Fisher Scientific). The three final solutions were 0.1 mg/mL SLS, 0.1 mg/mL collagen with 0.278 mg/mL SLS, and 0.1 mg/mL collagen. Collagen samples were incubated overnight at 37 °C prior to TEM. Samples were then vortexed for 10 s and sonicated for 5 min prior to being applied to the TEM grids. Carbon-coated 300 mesh copper grids (cat. no. CF300-CU, Electron Microscopy Sciences) were glow discharged, and then 5 μL of sample was applied for 5 min; excess moisture was removed using filter paper. The SLS samples were stained with 3% phosphotungstic acid (PTA, pH 5, cat. no. 19502-3, Electron Microscopy Sciences, >93.7%), with a contact time of 5 min, again removing excess moisture with filter paper. The collagen samples were stained with uranyl acetate solution (UA, cat. no. 22400, Electron Microscope Sciences, >92.4%), with a contact time of 2 min. Collagen−SLS composite samples were stained with UA, also for 2 min. The samples were then viewed using a JEOL-1400 Biological and Soft Material TEM at LSU Shared Instrumentation Facility (SIF).

Formation of Collagen−Lignin Composites. Collagen−lignin composites were prepared by diluting stock Col I (cat. no. 354249, Corning) and SLS (2.5, 5.0, or 10.0 mg/mL final concentration) to achieve a final collagen concentration of 3.5 or 1.8 mg/mL with 17 mM acetic acid (cat. no. A38S-212, Fisher Scientific, 99.7%). Collagen−lignin composites were neutralized in a 10× buffer solution with final concentrations of 23 mM HEPES (cat. no. AC215000250, Acros Organics, 99%), 10 mM sodium hydroxide (NaOH, cat. no. S8045-500G, Sigma-Aldrich, 98%), 44 mM sodium bicarbonate ($NaHCO_3$, cat. no. AC217125000, ACROS Organics, 99.5%), and 1× phosphate buffer saline (PBS, cat. no. BP399-4, Fisher Scientific). To prepare collagen−lignin composites with monolignols, individual monolignols were first added to methanol to create supersaturated solutions, 10 000 coniferyl (G), 20 000 sinapyl (S), and 30 000 coumaryl (H) mg/mL, and then added to the buffer solution, achieving a concentration of 50 mg/mL. Monolignol buffer solution was then added to the collagen to achieve a final monolignol concentration of 5.0 mg/mL. To prepare collagen−lignin composites with alkali-extracted lignin, each extracted lignin was added to 17 mM acetic acid solution and then mixed with collagen to achieve a final concentration of 5.0 mg/mL.

2D Cytotoxicity of Collagen−SLS Composites. Human adipose-derived stromal cells[28] (ASC, LaCell, LLC) were used to test the cytotoxicity of collagen−SLS composites. ASCs were seeded in a 96-well plate at a 3100/cm^2 seeding density. Collagen−SLS composites were prepared as previously described for TEM imaging. The final concentrations for the solutions were as follows: 1× buffer, 0.278 mg/mL SLS, 0.1 mg/mL collagen, and 0.1 mg/mL collagen with 0.278 mg/mL SLS. Prepared solutions were then pipetted over ASC monolayers and allowed to incubate overnight. Controls for the experiment included cells with media and media with no cells. Cell-counting kit 8 (CCK8, cat. no. CK04-05, Dojindo) was used to assess cell viability. Samples were washed with PBS and incubated with the culture medium and CCK8 for 2 h. The solutions were then

DOI: 10.1021/acsabm.9b00444
ACS Appl. Bio Mater. 2019, 2, 3562−3572

transferred to a new 96-well plate, and the absorbance was read at 450 nm with a Cytation3 (Biotek) spectrophotometer.

Live/Dead Staining in 3D Collagen−SLS Composites. Agarose molds were prepared to house collagen−SLS composites to test the viability of human ASCs and murine embryonic stem cells (ESCs).[29] An agarose (cat. no. RC-122, G Biosciences, 100%) solution was prepared at a 10 mg/mL concentration in PBS and heated until clear. Molds were prepared in 24-well plates using custom 3D printed inserts that created a cylindrical void 8 mm in diameter, and they are referred to as agarose cups. Once the molds cooled at RT and became translucent, they were covered in 1% antibiotic/antimycotic solution (cat. no. 15240-062, ThermoFisher) in PBS, for at least 24 h at 4 °C. Collagen−SLS composites were prepared (see Formation of Collagen−SLS Composites) and placed into the agarose cups prior to seeding (3000 cells/cm^2 for both stem cells). To test viability of ASCs and ESCs in 3D collagen−SLS composites, the live/dead staining assay (cat. no. 30002-T, Biotium) was utilized. At days 1 and 7, hydrogels were washed three times with 1× PBS, transferred to a 48-well plate, and suspended in Calcein AM/EthDIII solution for 30 min at 25 °C. After 30 min, samples were removed from solution, washed with warm PBS three times, imaged using an inverted fluorescence microscope (Nikon Eclipse Ti2), and NIS Elements Advanced Research Microscope Imaging Software (NIS Elements AR, Nikon).

Immunogenicity of Collagen−SLS Composites. Standards and working solutions were prepared following the Pierce LAL (limulous amoebocyte lysate) Chromogenic Endotoxin Quantitation Kit (cat. no. 88282, Thermo Scientific) protocol. All samples were assayed for endotoxin and were found to be below 0.06 EU/mL. All animal experiments were conducted under approved protocols from the Institution Animal Care and Use Committee (IACUC) at the University of Texas Medical Branch. BALB/c mice (5−6 weeks old Taconic Farms) were used to investigate the immunogenicity of collagen and SLS composites. Samples were dissolved in the sterilized neutralization buffer, and final immunization concentrations were the same as used for TEM. Mice were immunized subcutaneously with 100 μL of collagen, SLS, or collagen−SLS composite solutions and boosted 4 weeks later with half the dose. Negative control mice received injections of sterile neutralization buffer. Mice were sacrificed 2 weeks after the boost and sera were collected. To analyze antibody responses, solutions of collagen, SLS, or collagen−SLS composites were adsorbed onto high-binding ELISA plates overnight at 4 °C (20 μg/mL, 100 μL/well) and blocked with 1% BSA in PBST (0.5% (v/v) Tween 20 in PBS). Diluted sera (1:100, 100 μL/well) was applied for 1 h, and bound IgG was detected using peroxidase-conjugated goat antimouse IgG (H+L) (Jackson Immuno Research 1:5000, 100 μL/well). Plates were developed using the TMB substrate (eBioscience, 100 μL/well), and the reaction was stopped using 1 M phosphoric acid (50 μL/well). The plates were read at 450 nm, and the background absorbance from control wells was subtracted. Plates were washed in between steps 3 times with PBST.

RESULTS

SLS Exhibited Distinct Profiles of Molecular Weight Distribution and Chemical Natures from Alkali-Extracted Lignins. Insight into the size of molecules within each lignin type was obtained through the examination of molecular weight (M_w) distributions. $\overline{M}_w$ (weight-average molecular weight), $\overline{M}_n$ (number-average molecular weight), and polydispersity index (PDI) were estimated by GPC (Figure 1 and Table 1). The M_w distribution curves of SG, P, and PL showed major peaks around 2400 g/mol, while SLS was around 260 g/mol (Figure 1). Interestingly, despite SG having the largest M_w estimated as around 5400 g/mol, SG also showed a secondary peak that aligned with SLS, indicating a large percentage of low M_w compounds in SG that are similar in size to SLS. SLS showed the lowest $\overline{M}_w$ (460 g/mol) and $\overline{M}_n$ (280 g/mol), suggesting that SLS experienced the greatest degree of lignin depolymerization. The presence of the peak correlated to an increase in PDI of SG, which indicates a greater dispersity in the M_w distribution. Additionally, the low PDIs of SLS and PL indicated a narrower range of M_w distribution, while the PDI of P showed significantly larger M_w distribution, as evidenced in Table 2.

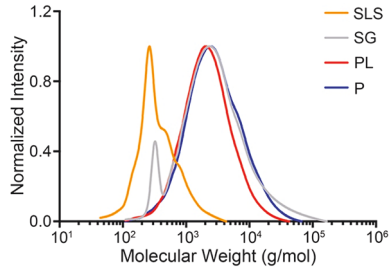

Figure 1. Molecular weight distribution of alkali-extracted lignins and SLS by GPC. Weight-averaged and number-average molecular weights and respective PDI are reported in Table 2. The M_w distribution of SG and SLS showed that the secondary peak of SG and the primary peak of SLS are overlapped around 250−300 g/mol.

Table 1. Summary of Sample Abbreviation

sample abbreviation	sample full name
SLS	sodium lignosulfonate
SG	switchgrass akali-extracted lignin
PL	poplar akali-extracted lignin
P	pine akali-extracted lignin
SLS−PLGA	sodium lignosulfonate-poly(lactic-*co*-glycolic acid) nanoparticles
C1.8	collagen type I at 1.8 mg/mL
C3.5	collagen type I at 3.5 mg/mL
C1.8L5.0	collagen type I at 1.8 mg/mL with 5.0 mg/mL SLS
C3.5L5.0	collagen type I at 3.5 mg/mL with 5.0 mg/mL SLS
C1.8PL5.0	collagen type I at 1.8 mg/mL with 5.0 mg/mL PL
C1.8P5.0	collagen type I at 1.8 mg/mL with 5.0 mg/mL P
C1.8SG5.0	collagen type I at 1.8 mg/mL with 5.0 mg/mL SG
C1.8L(1:X)	collagen type I at 1.8 mg/mL with SLS nanoparticles (1:*X*, where *X* is a ratio of PLGA to SLS) 5.0 mg/mL
C1.8G5.0	collagen type I at 1.8 mg/mL with 5.0 mg/mL coniferyl monolignol
C1.8S5.0	collagen type I at 1.8 mg/mL with 5.0 mg/mL sinapyl monolignol
C1.8H5.0	collagen type I at 1.8 mg/mL with 5.0 mg/mL *p*-courmaryl monolignol

Table 2. GPC of Alkali-Extracted Lignins and SLS

lignin	M_w (g/mol)	M_n (g/mol)	$PDI_{polymer}$ (M_w/M_n)
poplar (PL)	3100	1900	1.63
pine (P)	4500	1800	2.50
switchgrass (SG)	5400	1400	3.86
SLS	460	280	1.64

The chemical and structural profile of the extracted P, PL, SG, and SLS were examined by Fourier transform infrared (FT-IR) spectroscopy. Eight peaks were analyzed to compare the chemical signatures of lignins and to examine the presence of residual sugars (Figure 2a−d and Table 3).

The peak at 1510 cm^{-1} represents the aromatic skeleton of lignin, shown in all alkali-extracted lignins except SLS. The peaks at 1218 and 1268 cm^{-1} represented the C−O vibration

DOI: 10.1021/acsabm.9b00444
ACS Appl. Bio Mater. 2019, 2, 3562−3572

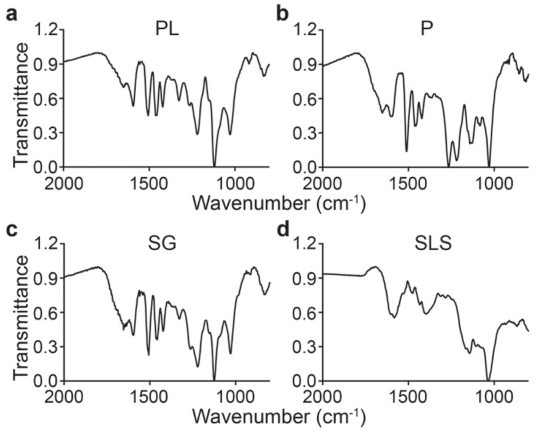

Figure 2. FTIR spectra of alkali-extracted lignins and SLS. All extracted lignins and SLS show the C−O vibration in the guaiacyl ring (G) as evidenced at 1218 and 1268 cm^{-1}, while the transmittance of SLS at this wavenumber is reduced. The peak at 1329 cm^{-1} representing the syringyl (S) and guaiacyl (G) condensed lignin is revealed in PL (a) and SG (c), while the transmittance of SLS (d) and P (b) at this wavenumber is also reduced.

Table 3. Compositional Analysis of Alkali-Extracted Lignins

lignin	% glucan[a]	% xylan[a]	% lignin[a]
poplar (PL)	2.01 ± 0.57	0	97.99 ± 0.57
pine (P)	6.35 ± 2.02	0.23 ± 0.12	93.43 ± 2.11
switchgrass (SG)	1.01 ± 0.16	0	98.99 ± 0.16

[a]Reported as mean ± standard deviation.

in the guaiacyl (G) ring[30] and were shown in all alkali-extracted lignins. However, these peaks were reduced in SLS, which could be attributed to the interference with S=O stretching that appears from 1155 to 1245 cm^{-1}.[30] The peak at 1329 cm^{-1} representing the syringyl (S) and G condensed lignin was revealed in PL and SG, while the intensity of this peak was small in both SLS and P. This reduction could be due to the low content of S, which is consistent with the nature of softwood lignins.[31,32] No significant peaks were detected at 900, 1056, 1098, and 1375 cm^{-1} in any of the lignin samples, representing the amorphous cellulose, C−O vibration of crystalline cellulose, C−O stretch in cellulose and hemicellulose, and C−H deformation in cellulose and hemicellulose, respectively.[33] These results indicated that no significant amount of sugars was present in any of the lignin samples, that all the alkali-extracted lignins showed similar composition, and that SLS and P showed to contain dominantly G lignin. To further verify the chemical information on the biomass feedstock composition, we analyzed the three most abundant cell wall components, glucan, xylan, and lignin using HPLC. Glucan and xylan are the major carbohydrates available for biomass conversion, while lignin is known to hinder access to carbohydrates.[34] As shown in Table 3, all of the extracted PL, P, and SG showed minimal to zero fraction of glucan and xylan, while the majority of recovered samples is composed of lignin.

Synthesis of SLS−PLGA Nanoparticles. To elucidate the physical interaction between collagen fibers and lignin nanoparticles, we functionalized PLGA nanoparticles with SLS, where the ratio of nanoparticle was varied from 1:1 to 1:8 (SLS:PLGA). As shown in Table 4, the SLS−PLGA nanoparticles appeared relatively monodispersed in comparison to

Table 4. DLS of SLS−PLGA Nanoparticles and SLS (n = 3)[a]

SLS/PLGA ratio	average diameter ± st. dev. (nm)	PDI_{DLS} (st. dev./mean dia.)^2
1:1	105.7 ± 0.6	0.258 ± 0.023
1:2	130.9 ± 0.6	0.282 ± 0.018
1:4	182.0 ± 2.1	0.243 ± 0.015
1:8	202.4 ± 3.1	0.221 ± 0.024
SLS	120.2 ± 6.1	0.469 ± 0.108

[a]Abbreviations: dia., diameter; st. dev., standard deviation.

that of SLS. While PLGA nanoparticles are water-insoluble as evidenced by phase separation, SLS−PLGA nanoparticles were water-soluble in the buffers that were used to prepare collagen−nanoparticle composites.

We further confirmed the conjugation of lignin to PLGA by FT-IR and nuclear magnetic resonance (NMR) spectroscopy. The FT-IR spectrum of SLS−PLGA in Figure 3 showed

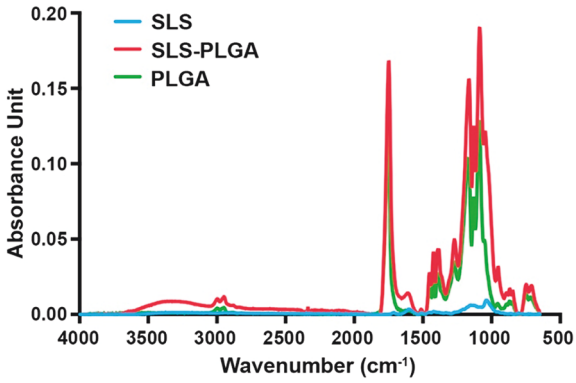

Figure 3. FT-IR spectra of SLS, PLGA, and SLS−PLGA. The absorption peaks at 1598 and 1511 cm^{-1} correspond to the vibrations of aromatic rings (α-carbonyl groups) characteristics of lignin. The absorption peak at 1037 cm^{-1} is associated with the primary and secondary alcohol groups of lignin.

absorption peaks at 1598 and 1511 cm^{-1}, corresponding to the vibration of aromatic rings (α-carbonyl groups) of SLS. The absorption peak at 1037 cm^{-1} is associated with the primary and secondary alcohol groups of SLS.

The ^{1}H NMR spectrum of SLS−PLGA in Figure 4 showed the chemical shifts between 3.5−4.0 ppm, indicative of the protons in methoxyls. The chemical shifts from 6.20−6.80 ppm were attributed to S units and that between 6.80 and 7.20 ppm was attributed to aromatic protons in G units in SLS.[35,36] The chemical shifts at 4.35−4.75 ppm and 4.75−5.00 ppm were assigned to the protons in β-O-4′ units, at 5.45−5.75 ppm to the protons in β-5 structures, and at 5.75−6.20 ppm to the protons in β-O-4′ and β-1′ structures, respectively (Figure S1, Supporting Information).[37]

Lignosulfonate including 5 mg/mL Attenuated Shear Thinning of Collagen Matrix and Significantly Increased Shear Moduli Around 10-Fold. Collagen−SLS composites exhibited significant attenuation of shear thinning over the range of frequencies (Figure 5). The collagen−SLS composite of 1.8 mg/mL Col I and 5.0 mg/mL SLS (L) (C1.8L5) exhibited the highest degree of stiffening with the storage modulus (G'), increasing approximately 10-fold (~670 Pa) compared to the collagen-only (C1.8) control as evidenced in Figure 5a. In addition, loss (G'') moduli were

DOI: 10.1021/acsabm.9b00444
ACS Appl. Bio Mater. 2019, 2, 3562−3572

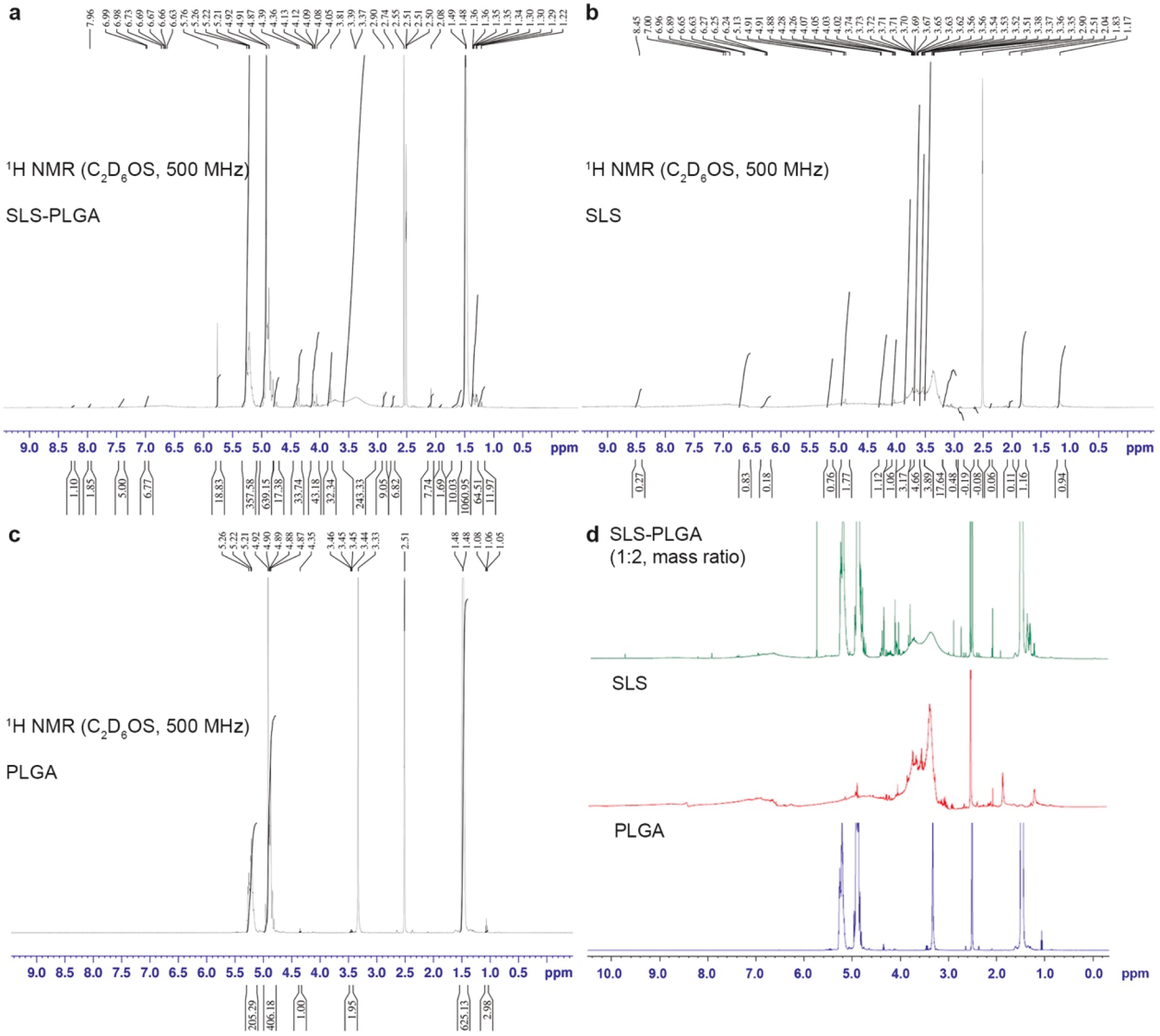

Figure 4. Individual ^{1}H NMR spectrum of SLS−PLGA (a), SLS (b), and PLGA (c) with peak integration and chemical shift values. (d) Consolidated ^{1}H NMR spectra of SLS−PLGA, SLS, and PLGA for comparison.

also increased around 9-fold. In contrast, the collagen−SLS composite of 3.5 mg/mL Col I and 5.0 mg/mL SLS (C3.5L5) showed around a 2-fold (~400 Pa) increase of storage modulus (G') in comparison to the collagen control (C3.5) (Figure 5b). As the collagen fiber density increased, the impact of polymeric lignin particles to the viscoelasticity of collagen−SLS composites was diminished. Furthermore, this specific 5 mg/mL of SLS enhanced the shear moduli of collagen−SLS composites most synergistically, while 2.5 (C1.8L2.5) and 10 (C1.8L10) mg/mL of SLS in collagen−SLS composites drastically reduced the storage (G') and loss (G'') moduli when compared to collagen-only composites (Figure S2, Supporting Information). The C1.8L5 collagen−SLS composites exhibited the most synergistic enhancement of shear moduli and thus, this specific formulation was used for all subsequent studies.

Alkali-Extracted Lignin from Switchgrass Increased the Stiffness of Collagen−Lignin Composites and Attenuated Shear-Thinning Properties. The composition and structure of lignin vary significantly when examining different biomass feedstocks. These differences in monolignol G, S, and H (*p*-hydroxyphenyl) content afford different lignin properties where higher S ratios reduce lignin branching by impeding β-5 and/or 5−5 linkages[31] (Figure S1, Supporting Information), which makes hardwood lignin have more of a linear structure as compared to softwood lignin. Additionally, the high amount of C−C linkages makes the softwood lignin more condensed and resistant to degradation due to the bond dissociation energy required to break C−C linkages (β-5) compared to ether linkages (β-O-4′).[38,39] Grasses contain all three types of monolignols (H, S, and G lignin), which is considered less recalcitrant than softwoods.[32] In this study, we tested lignins extracted from three different feedstocks that were processed under identical alkaline pretreatment conditions to observe the viscoelastic response in collagen composites. Pine (P), poplar (PL), and switchgrass (SG) all exhibited varying levels of improvement of both storage (G') and loss (G'') moduli (Figure 6). SG composites exhibited the most significant improvement on shear moduli (both G' and G'') and the attenuation of shear thinning of the collagen−lignin composites as shown in Figure 6c. Comparison of shear moduli at 6.28 rad/s showed that storage (G') and loss (G'') of

DOI: 10.1021/acsabm.9b00444
ACS Appl. Bio Mater. 2019, 2, 3562−3572

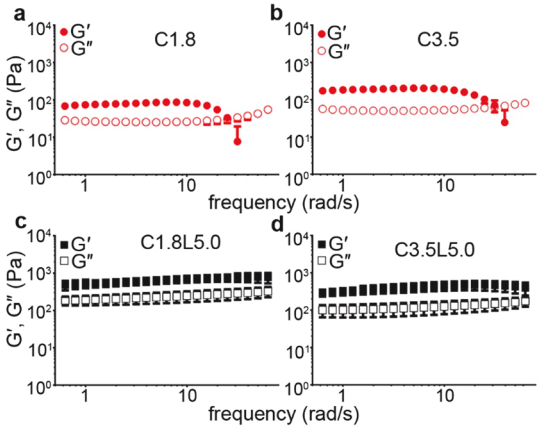

Figure 5. Storage (G') and loss (G'') moduli of collagen−SLS composites by frequency sweeping from 0.628 to 62.8 (rad/s) at 10% strain. (a) C1.8, collagen 1.8 mg/mL; (b) C3.5, collagen 3.5 mg/mL; (c) C1.8L5.0, collagen 1.8 mg/mL with SLS 5.0 mg/mL; (d) C3.5L5.0, collagen 3.5 mg/mL with SLS 5.0 mg/mL. mean ± SD, n = 4.

SG were significantly different from those of collagen-only composites, as evidenced in Figure S3a (Supporting Information). Although collagen−SG lignin composites enhanced mechanical properties, the extent of enhancement of collagen−SLS was much more significant (Figure S3a, Supporting Information). As discussed earlier, thus, we decided to use C1.8L5.0 (Figure 5c) to test the structural and biological responses.

SLS−PLGA Nanoparticles Did Not Modulate Mechanical Properties of Collagen Type I. In oscillating rheometry, all collagen−lignin composites including SLS−PLGA nanoparticles showed no significantly different storage (G') and loss (G'') moduli from collagen-only composites (Figure 7 and Figure S3b in Supporting Information). To assess the average diameter of SLS−PLGA nanoparticles, we performed DLS and the results are presented in Table 4. The average diameters of 1:1 and 1:2 SLS−PLGA nanoparticles are 105.7 ± 0.6 nm and 130.9 ± 0.6 nm, respectively. The average diameter of SLS is 120.2 ± 6.1 nm (Table 4). These results indicate that the nature of SLS and its specific interaction with collagen fibers are the key element to stiffen the collagen−lignin composites and that similar sized SLS−PLGA nanoparticles did not significantly alter the mechanical properties of collagen−nanoparticle composites prepared with SLS−PLGA nanoparticles.

Monolignols Have Minimal Impact on the Stiffness of Collagen−Lignin Composites. Monolignols G, S, and H (Figure 8e) were incorporated to form collagen−lignin composites to determine if the different functional groups of monolignols interact preferentially with collagen fibers to improve the overall stiffness. Collagen−monolignol composites exhibited no statistically significant difference of respective storage (G') and loss (G'') moduli in comparison to collagen-only composite (Figure S3c, Supporting Information). Of the three monolignols, S incorporated collagen−composites enhanced storage modulus and attenuated the shear-thinning profile at higher frequencies (Figure 8b). As shown in Figure 8e, the dimethoxy group in S potentially conferred stiffening of collagen−sinapyl composites, but this mechanistic understanding needs further experiments to confirm the specific interaction of dimethoxy groups and functional groups of Col I.

Distinct Col I Fibril and SLS Association Was Evidenced by TEM. In order to observe the physical interaction between collagen fibril and SLS, we performed TEM with collagen, collagen−SLS, and SLS samples. As evidenced by electron micrographs (Figure 9a,b), the SLS nanoparticle size was approximately 120 nm, which was similar to the size of the SLS−PLGA nanoparticles (from 106 to 202 nm by DLS measurement as indicated in Table 4). TEM micrographs showed that SLS particles were associated within the collagen fibrils (Figure 9c,d, indicated with ▲). The collagen−SLS fibril bundles exhibited a tighter and more compact structure than collagen-only fibril bundles (Figure 9e,f).

Collagen−SLS Composites Were Minimally Cytotoxic and Immunogenic. To assess the potential of scaffolds for tissue regeneration, the cytotoxicity of collagen−SLS composites was tested in 2D and 3D cultures. Lignins including SLS showed cytotoxic effects, but only at very high concentrations around 0.7−1.2 mg/mL to 3T3 fibroblasts.[40,41] Lignins extracted from *Acacia nilotica* showed a higher cytotoxic potential toward the MCF-7 breast cancer cell line, while being only slightly toxic to human hepatic stellate cells.[42] However, these cell lines are less relevant to regenerative medicine applications than stem cells, thus we tested our collagen−SLS composites with ASCs and ESCs. We applied our collagen−SLS composites onto ASC cultures in 2D layers to directly observe the impact of material toxicity within cells. The results presented in Figure 10a showed the cytotoxicity of collagen−SLS composites were comparable to all other groups of samples including buffer-only and collagen-only composites in 2D cultures. Collagen−SLS composites did not induce a reduction of ASC viability in 2D cultures, indicating the collagen−SLS composites are noncytotoxic to ASCs in 2D culture conditions. ASCs or ESCs were also applied to 3D

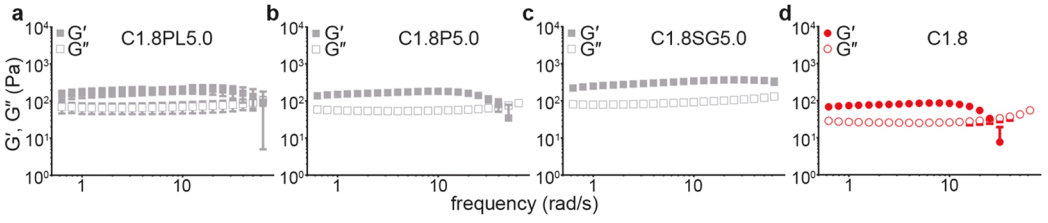

Figure 6. Storage (G') and loss (G'') moduli of collagen−lignin composites by frequency sweeping from 0.628 to 62.8 (rad/s) at 10% strain with alkali-extracted lignins. (a) C1.8PL5.0, collagen 1.8 mg/mL with poplar lignin (PL) 5.0 mg/mL; (b) C1.8P5.0, collagen 1.8 mg/mL with pine (P) lignin 5.0 mg/mL; (c) C1.8SG5.0, collagen 1.8 mg/mL with switchgrass lignin (SG) 5.0 mg/mL; (d) C1.8, collagen 1.8 mg/mL, mean ± SD, n = 4.

DOI: 10.1021/acsabm.9b00444
ACS Appl. Bio Mater. 2019, 2, 3562−3572

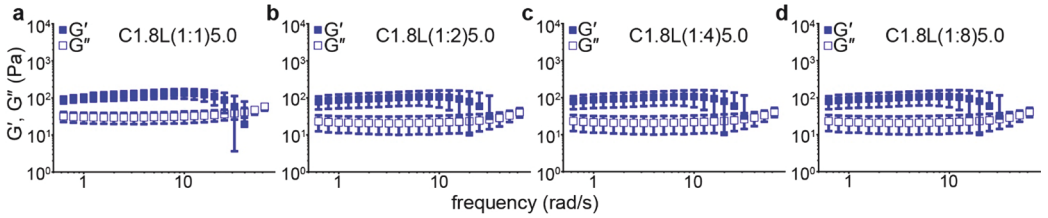

Figure 7. Storage (G') and loss (G'') moduli of collagen−nanoparticle composites with SLS−PLGA by frequency sweeping from 0.628 to 62.8 (rad/s) at 10% strain. (a−d) C1.8L (1:X), collagen 1.8 mg/mL with SLS nanoparticles (1:X, where X is a ratio of PLGA to SLS) 5.0 mg/mL. Mean ± SD, n = 4.

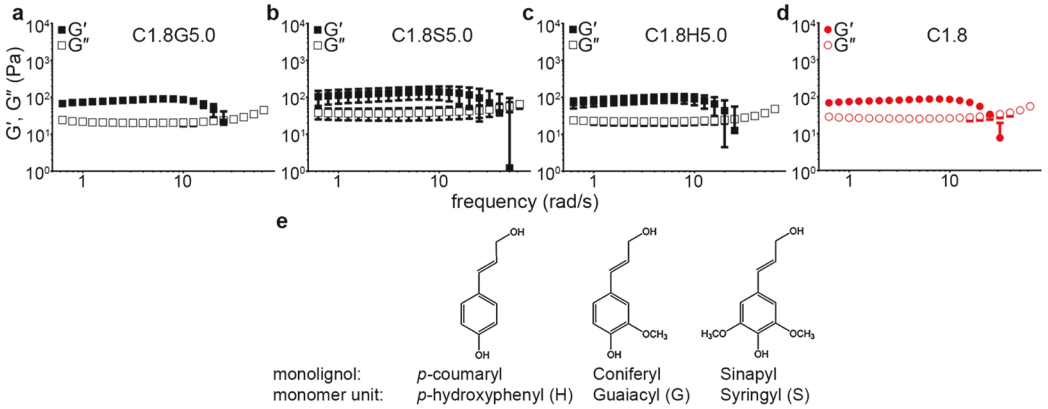

Figure 8. Storage (G') and loss (G'') moduli of collagen−lignin composites by frequency sweeping from 0.628 to 62.8 (rad/s) at 10% strain with monolignols. (a) C1.8G5.0, collagen 1.8 mg/mL with G monolignol 5.0 mg/mL; (b) C1.8S5.0, collagen 1.8 mg/mL with S monolignol 5.0 mg/mL; (c) C1.8H5.0, collagen 1.8 mg/mL with H monolignol 5.0 mg/mL; (d) C1.8, collagen 1.8 mg/mL, mean ± SD, n = 4; (e) molecular structures of monolignols.

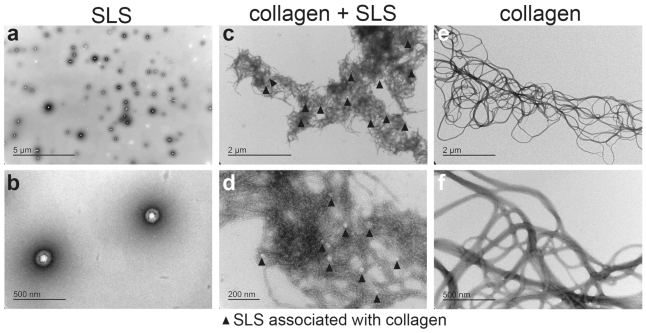

Figure 9. Transmission electron micrographs of SLS in solution (0.1 mg/mL, negative staining with 3% PTA negative stain (a and b). Collagen−SLS composite in solution, 0.1 mg/mL + 0.278 mg/mL, using a UA stain (c and d). Collagen fibrils in solution, 0.1 mg/mL, using a UA stain (e and f).

collagen−SLS and collagen-only composites. As shown in Figure 10b, live/dead staining of ASCs or ESCs in both collagen−SLS and collagen-only composites exhibited only a few dead cells after 7 days of culture. These results indicated that the viability of either ASCs or ESCs was well maintained in both 3D collagen−SLS and collagen-only composites at similar levels. In addition, the expression of pluripotency genes (Nanog, Sox2, and Pou5f1/Oct4) of ESCs was maintained over 7 days in collagen−SLS composites (Figure S4, Supporting Information). The potential use of the collagen−SLS composite is intended not only for 3D *in vitro* culture but also for *in vivo* tissue repair. Thus, we tested the immunogenicity of collagen−SLS composites by injecting the matrix biomaterials that we tested *in vitro* into BALB-c mice. After 5 weeks, the mice experienced very low levels of IgG titer for all of the matrix biomaterials injected, but only the SLS solution showed a significant difference between the buffer solution ("SLS" in Figure 10c), but this was due to one high titer response in the group. The titer results presented in Figure 10c indicated the immunogenicity of collagen−SLS composites was also not significantly different from collagen-only composites. These results indicated that collagen−SLS composites were noncytotoxic to ASCs, supported the growth of ASCs and ESCs in 3D cultures, and showed minimal immunogenicity over 5 weeks, exhibiting the potential of an engineered matrix for tissue repair and regeneration with ASCs and ESCs.

DISCUSSION

Incorporation of native ECM proteins is critical when attempting to create an *in vitro* culture platform or *in vivo* tissue replacement. Transitioning from 2D to 3D culture is challenging because most ECM proteins exhibit limited capability of forming robust scaffolds without a means of cross-linking or forming composites.[14,43] To compensate the mechanical properties of ECM-only matrices, previous reports showed to create composites with synthetic polymers or other ECM proteins. For example, synthetic poly(ethylene glycol) (PEG)-based scaffolds encapsulated human ES-derived MSCs[44] with ECM proteins (collagen type I, fibronectin, or laminin-111), while maintaining mechanical properties of the ECM scaffolds.[14] In contrast, collagen-only matrices exhibit varying levels of stiffness ranging from 0.01−10 kPa depending on concentration and method of cross-linking.[10,45] There are a number of different methods to cross-link collagen matrices

DOI: 10.1021/acsabm.9b00444
ACS Appl. Bio Mater. 2019, 2, 3562−3572

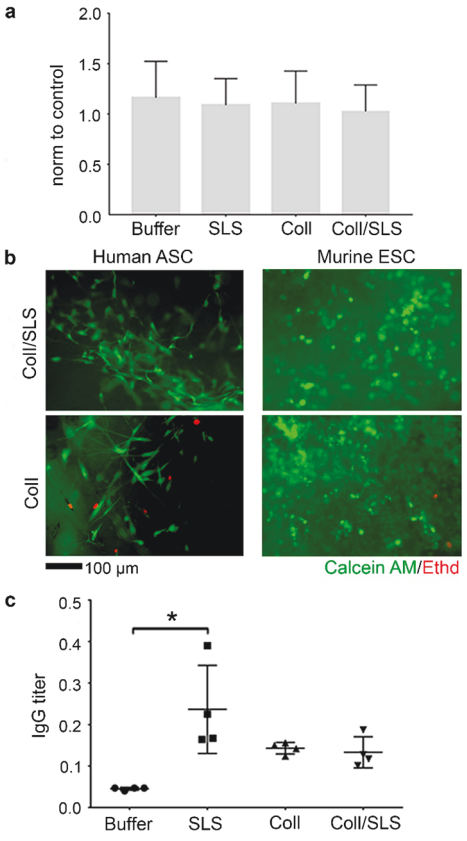

Figure 10. Cytotoxicity and immunogenicity of collagen−SLS composites. (a) Concentrations of samples were 0.278 mg/mL lignin, 0.1 mg/mL collagen, and 0.1 mg/mL collagen with 0.278 mg/mL SLS, mean ± SD, $n = 3$. Samples were diluted in media and applied to 2D cultures of ASCs, 3125 cell/cm^2. Media controls were subtracted as background, and resulting data were normalized to the cell control. (b) Live (green)/dead (red) staining of 3D composites seeded with ASCs or ESCs and cultured for 7 days. (c) BALB/c mice were injected with 1× buffer solution, 0.278 mg/mL SLS solution, 0.1 mg/mL collagen solution, and 0.1 mg/mL collagen with 0.278 mg/mL SLS. After 5 weeks, the mice were sacrificed, their sera were collected, and anti-ECM IgG was detected in the sera using ELISA, mean ± SD, $n = 4$, ANOVA post hoc Tukey's test, $^*p < 0.05$.

and each method is with their own benefits and drawbacks. Chemical cross-linking allows to form stiff scaffolds but can also lead to cytotoxicity and/or immunogenicity with the selected methods[6−11] from byproducts, radicals, or uncross-linked monomers. To avoid cytotoxicity, immunogenicity, and potential compositional drift from covalent cross-linking,[46] we sought physical co-assembly with Col I. Here, we also incorporated a structural matrix component found in plant cell walls,[47] namely lignin, that can enhance mechanical properties of collagen-based matrices and confer other beneficial properties to collagen-based matrices for cell and tissue scaffolds. As shown in Figure 5, the collagen−SLS composites showed the increase of mechanical properties, around 10-fold, in comparison to the collagen-only composites without introducing any cross-linking chemistry or additional treatment. With the dramatic enhancement of the mechanical properties by simply adding SLS, future directions need to examine incorporation of other ECM proteins to enhance or modulate biofunctionality by including hyaluronic acid, glycoproteins (e.g., laminin, fibronectin, vitronectin, etc.), and proteoglycans.

Inspired by the complex structures and the structural roles in plant tissues, we hypothesized that the complex nature of lignin provides the enhancement of mechanical properties to collagen composites without the need for toxic cross-linkers, photo-initiators, or other molecules previously used in collagen cross-linking.[6−11] SLS is widely used as a water reducer (plasticizer) to enhance concrete strength in the construction field thanks to generating electrostatic repulsion, steric hindrance or lubrication among particles.[48] Ironically, C1.8L5 composites did not enhance fluidity, but attenuated the shear-thinning property. In contrast, a smaller (2.5 mg/mL) or higher (10 mg/mL) amount of SLS with 1.8 mg/mL of Col I exhibited different mechanical properties (as shown in Figure S2 in Supporting Information) from C1.8L5 collagen−SLS composite. We hypothesized that catechol-like polyaromatic structures will enhance mechanical properties via noncovalent interactions between SLS and collagen fibrils. However, the increase of stiffness was not linearly proportional to the concentration of incorporated SLS. Rather, one particular concentration at 5 mg/mL of SLS showed the stiffening and attenuation of shear thinning. Similar behaviors were observed in suspension rheology reported by Koos and Willenbacher.[49] When solid particles are dispersed in a fluid, adding small amount of a secondary fluid that is immiscible with the continuous phase of the suspension causes agglomeration due to capillary forces and creates particle networks. This alters the bulk rheological behavior from weakly elastic to gel-like structures. In our case, SLS particles are dispersed in the aqueous buffer and collagen fibrils are inherently immiscible in the aqueous phase. When the collagen solution is added to SLS in the aqueous buffer, collagen fibrils and SLS presumably form networks via hydrogen bonding (more likely) or $\pi-\pi$ stacking (less likely due to the fact that majority of amino acids in Col I are glycine, proline and hydroxyproline).[50] These interactions prevent sliding of collagen fibrils in the collagen−SLS composites, resulting in the significant increase of shear modulus with relatively small amount of collagen (0.18% w/v or 1.8 mg/mL).[49] Although this phenomenon explains the increase of shear modulus, further microscopic analysis is warranted to confirm the pendular or capillary state of network formation. Nonetheless, this specific type of interaction of collagen−SLS warrants further investigation of lignin composition in collagen-based hydrogels. Although the mechanical property data showed that lignin, especially SLS, is a synergistic enhancer for collagen gels, the physical coassembly of collagen−lignin composites still exhibited some extent of variability in comparison to chemoselective chemistry.[13,14,51−53] To avoid such variability in preparing composites, future work may need to include composites created via a chemoselective cross-linking of lignin with other matrix biomaterials including collagen, gelatin or hyaluronic acid.

CONCLUSIONS

Inspired by polyphenolic structures of lignin, we attempt to modulate mechanical properties of collagen−lignin composites for *in vitro* scaffolds and *in vivo* tissue repairs. We showed that SLS and SG lignin, out of multiple lignin candidates, significantly enhanced both storage and loss moduli in comparison to the collagen-only composite. From the results of TEM and oscillating rheometry with SLS−PLGA composites, this enhancement of stiffness and attenuation of shear-thinning properties was primarily due to the interaction between SLS and Col I. Inclusion of the alkali-extracted lignin

DOI: 10.1021/acsabm.9b00444
ACS Appl. Bio Mater. 2019, 2, 3562−3572

from SG showed similar profiles of storage and loss moduli to those of SLS, but the extent of enhancement was still lower than that of SLS. From GPC analyses, smaller M_w species found around 250−300 g/mol were common to SLS and SG. Using FTIR spectroscopy, SLS contains primarily G lignin devoid of any significant polysaccharide. To apply this collagen−SLS composite for tissue repair, we tested cytotoxicity with stem cells and immunogenicity in BALB/c mice, which were shown to be minimal and comparable to the collagen-only controls. In the future, this simple, physical coassembling method can be applied to produce engineered matrices without introducing complex cross-linking chemistry.

■ ASSOCIATED CONTENT

Supporting Information

The Supporting Information is available free of charge on the ACS Publications website at DOI: 10.1021/acsabm.9b00444.

Detailed information of monolignol synthesis, cultures of ASC and ESCs, and bacterial endotoxin test (PDF)

■ AUTHOR INFORMATION

Corresponding Authors

*E-mail: j.shi@uky.edu.

*E-mail: jjung1@lsu.edu.

ORCID

Bert C. Lynn: 0000-0001-8426-3024

Jian Shi: 0000-0003-3022-4446

Jangwook P. Jung: 0000-0001-5783-4549

Present Address

‖J.S.R.: Biomedical Engineering, Washington University in St. Louis, Whitaker Hall, 390B, St. Louis, Missouri 63130, USA.

Author Contributions

J.P.J. and J.S. conceived the experiments. J.A.B., S.A.Z., and J.C.P. prepared collagen−lignin composites for all experiments. C.E.A. synthesized and characterized nanoparticles. R.M.K. and B.C.L. prepared and characterized alkali-extracted lignins and monolignols, respectively. J.S.R. conducted immunogenicity experiments, and K.M.H. maintained cell cultures.

Notes

The authors declare no competing financial interest.

■ ACKNOWLEDGMENTS

The authors acknowledge the support from the National Science Foundation EPSCoR (Track 2 RII, OIA 1632854, J.A.B., C.E.A., B.C.L., R.M.K., J.S., and J.P.J.) and REU EEC (1560305, J.C.P.). This work was supported by startup funding from the Department of Biological and Agricultural Engineering (J.P.J.).

■ REFERENCES

(1) Chevallay, B.; Herbage, D. Collagen-based Biomaterials as 3D Scaffold for Cell Cultures: Applications for Tissue Engineering and Gene Therapy. *Med. Biol. Eng. Comput.* **2000**, *38* (2), 211−218.

(2) Cukierman, E.; Pankov, R.; Stevens, D. R.; Yamada, K. M. Taking Cell-Matrix Adhesions to the Third Dimension. *Science* **2001**, *294* (5547), 1708−1712.

(3) Rhee, S.; Grinnell, F. Fibroblast Mechanics in 3D Collagen Matrices. *Adv. Drug Delivery Rev.* **2007**, *59* (13), 1299−1305.

(4) Reese, S. P.; Ellis, B. J.; Weiss, J. A. Micromechanical Model of a Surrogate for Collagenous Soft Tissues: Development, Validation and Analysis of Mesoscale Size Effects. *Biomech. Model. Mechanobiol.* **2013**, *12* (6), 1195−1204.

(5) Brown, R. A. IntThe Beginning There Were Soft Collagen-Cell Gels: Towards Better 3D Connective Tissue Models? *Exp. Cell Res.* **2013**, *319* (16), 2460−2469.

(6) Mason, B. N.; Starchenko, A.; Williams, R. M.; Bonassar, L. J.; Reinhart-King, C. A. Tuning Three-Dimensional Collagen Matrix Stiffness Independently of Collagen Concentration Modulates Endothelial Cell Behavior. *Acta Biomater.* **2013**, *9* (1), 4635−4644.

(7) Drzewiecki, K. E.; Parmar, A. S.; Gaudet, I. D.; Branch, J. R.; Pike, D. H.; Nanda, V.; Shreiber, D. I. Methacrylation Induces Rapid, Temperature-Dependent, Reversible Self-Assembly of Type-I Collagen. *Langmuir* **2014**, *30* (37), 11204−11211.

(8) Brinkman, W. T.; Nagapudi, K.; Thomas, B. S.; Chaikof, E. L. Photo-Cross-Linking of Type I Collagen Gels in the Presence of Smooth Muscle Cells: Mechanical Properties, Cell Viability, and Function. *Biomacromolecules* **2003**, *4* (4), 890−905.

(9) Peng, Y. Y.; Yoshizumi, A.; Danon, S. J.; Glattauer, V.; Prokopenko, O.; Mirochnitchenko, O.; Yu, Z.; Inouye, M.; Werkmeister, J. A.; Brodsky, B.; Ramshaw, J. A. A Streptococcus Pyogenes Derived Collagen-Like Protein as a Non-Cytotoxic and Non-Immunogenic Cross-Linkable Biomaterial. *Biomaterials* **2010**, *31* (10), 2755−2761.

(10) Raub, C. B.; Suresh, V.; Krasieva, T.; Lyubovitsky, J.; Mih, J. D.; Putnam, A. J.; Tromberg, B. J.; George, S. C. Noninvasive Assessment of Collagen Gel Microstructure and Mechanics Using Multiphoton Microscopy. *Biophys. J.* **2007**, *92* (6), 2212−2222.

(11) Khor, E. Methods for the Treatment of Collagenous Tissues for Bioprostheses. *Biomaterials* **1997**, *18* (2), 95−105.

(12) Yang, F.; Cho, S.-W.; Son, S. M.; Hudson, S. P.; Bogatyrev, S.; Keung, L.; Kohane, D. S.; Langer, R.; Anderson, D. G. Combinatorial Extracellular Matrices for Human Embryonic Stem Cell Differentiation in 3D. *Biomacromolecules* **2010**, *11* (8), 1909−1914.

(13) Jung, J. P.; Hu, D.; Domian, I. J.; Ogle, B. M. An Integrated Statistical Model for Enhanced Murine Cardiomyocyte Differentiation Via Optimized Engagement of 3D Extracellular Matrices. *Sci. Rep.* **2015**, *5*, 18705.

(14) Jung, J. P.; Bache-Wiig, M. K.; Provenzano, P. P.; Ogle, B. M. Heterogeneous Differentiation of Human Mesenchymal Stem Cells in 3D Extracellular Matrix Composites. *BioRes. Open Access* **2016**, *5* (1), 37−48.

(15) Feldman, D.; Wegener, G.; de Gruyter, W. Wood—chemistry, ultrastructure, reactions. *J. Polym. Sci., Polym. Lett. Ed.* **1985**, *23* (11), 601−602.

(16) Cybulska, I.; Brudecki, G.; Rosentrater, K.; Julson, J. L.; Lei, H. Comparative Study of Organosolv Lignin Extracted From Prairie Cordgrass, Switchgrass and Corn Stover. *Bioresour. Technol.* **2012**, *118*, 30−36.

(17) Contreras, S.; Gaspar, A. R.; Guerra, A.; Lucia, L. A.; Argyropoulos, D. S. Propensity of Lignin to Associate: Light Scattering Photometry Study with Native Lignins. *Biomacromolecules* **2008**, *9* (12), 3362−3369.

(18) Sarkanen, S.; Teller, D. C.; Abramowski, E.; McCarthy, J. L. Lignin. 19. Kraft Lignin Component Conformation and Associated Complex Configuration in Aqueous Alkaline Solution. *Macromolecules* **1982**, *15* (4), 1098−1104.

(19) Ross, K.; Mazza, G. Characteristics of Lignin from Flax Shives as Affected by Extraction Conditions. *Int. J. Mol. Sci.* **2010**, *11* (10), 4035.

(20) Mao, J. Z.; Zhang, L.; Xu, F. *Fractional and Structural Characterization of Alkaline Lignins from Carexmeyeriana Kunth* **2012**, *46*, 193−205.

(21) Waite, J. H.; Tanzer, M. L. Polyphenolic Substance of Mytilus Edulis: Novel Adhesive Containing L-Dopa and Hydroxyproline. *Science* **1981**, *212* (4498), 1038−1040.

(22) Lee, H.; Dellatore, S. M.; Miller, W. M.; Messersmith, P. B. Mussel-Inspired Surface Chemistry for Multifunctional Coatings. *Science* **2007**, *318* (5849), 426−430.

(23) Shi, J.; Ebrik, M. A.; Wyman, C. E. Sugar Yields from Dilute Sulfuric Acid and Sulfur Dioxide Pretreatments and Subsequent

DOI: 10.1021/acsabm.9b00444
ACS Appl. Bio Mater. 2019, 2, 3562−3572

Enzymatic Hydrolysis of Switchgrass. *Bioresour. Technol.* **2011**, *102* (19), 8930−8938.
(24) Xu, J.; Cheng, J. J.; Sharma-Shivappa, R. R.; Burns, J. C. Sodium Hydroxide Pretreatment of Switchgrass for Ethanol Production. *Energy Fuels* **2010**, *24* (3), 2113−2119.
(25) Selig, M. *Enzymatic Saccharification of Lignocellulosic Biomass Laboratory Analytical Procedure (LAP): issue date, 3/21/2008*. In Weiss, N., Ji, Y., Eds; National Renewable Energy Laboratory: CO, 2008.
(26) Selig, M.; Weiss, N.; Ji, Y. Enzymatic Saccharification of Lignocellulosic Biomass. NREL Laboratory Analytical Procedure. *Technical Report NREL/TP-510−42629*; National Renewable Energy Laboratory, CO. http://www.nrel.gov/docs/gen/fy08/42629.pdf: 2008.
(27) Lu, F.; Ralph, J. Derivatization Followed by Reductive Cleavage (DFRC Method), a New Method for Lignin Analysis: Protocol for Analysis of DFRC Monomers. *J. Agric. Food Chem.* **1997**, *45* (7), 2590−2592.
(28) Gimble, J. M.; Bunnell, B. A.; Guilak, F. Human Adipose-Derived Cells: An Update on the Transition to Clinical Translation. *Regener. Med.* **2012**, *7* (2), 225−235.
(29) Hsiao, E. C.; Yoshinaga, Y.; Nguyen, T. D.; Musone, S. L.; Kim, J. E.; Swinton, P.; Espineda, I.; Manalac, C.; deJong, P. J.; Conklin, B. R. Marking Embryonic Stem Cells with A 2A Self-Cleaving Peptide: A NKX2−5 Emerald GFP BAC Reporter. *PLoS One* **2008**, *3* (7), No. e2532.
(30) Xu, H.; Yu, G.; Mu, X.; Zhang, C.; DeRoussel, P.; Liu, C.; Li, B.; Wang, H. Effect and Characterization of Sodium Lignosulfonate on Alkali Pretreatment for Enhancing Enzymatic Saccharification of Corn Stover. *Ind. Crops Prod.* **2015**, *76*, 638−646.
(31) Liu, W.-J.; Jiang, H.; Yu, H.-Q. Thermochemical Conversion of Lignin to Functional Materials: A Review and Future Directions. *Green Chem.* **2015**, *17* (11), 4888−4907.
(32) Shi, J.; Pattathil, S.; Parthasarathi, R.; Anderson, N. A.; Kim, J. I.; Venketachalam, S.; Hahn, M. G.; Chapple, C.; Simmons, B. A.; Singh, S. Impact of Engineered Lignin Composition on Biomass Recalcitrance and Ionic Liquid Pretreatment Efficiency. *Green Chem.* **2016**, *18* (18), 4884−4895.
(33) Das, L.; Liu, E.; Saeed, A.; Williams, D. W.; Hu, H.; Li, C.; Ray, A. E.; Shi, J. Industrial Hemp as A Potential Bioenergy Crop in Comparison with Kenaf, Switchgrass and Biomass Sorghum. *Bioresour. Technol.* **2017**, *244*, 641−649.
(34) Payne, C. E.; Wolfrum, E. J. Rapid Analysis of Composition and Reactivity in Cellulosic Biomass Feedstocks with Near-Infrared Spectroscopy. *Biotechnol. Biofuels* **2015**, *8* (1), 43.
(35) Toledano, A.; Serrano, L.; Garcia, A.; Mondragon, I.; Labidi, J. Comparative Study of Lignin Fractionation by Ultrafiltration and Selective Precipitation. *Chem. Eng. J.* **2010**, *157* (1), 93−99.
(36) Zhou, H.; Yang, D.; Zhu, J. Y. Molecular Structure of Sodium Lignosulfonate from Different Sources and their Properties as Dispersant of TiO_2 Slurry. *J. Dispersion Sci. Technol.* **2016**, *37* (2), 296−303.
(37) Kubo, S.; Kadla, J. F. Poly(Ethylene Oxide)/Organosolv Lignin Blends: Relationship Between Thermal Properties, Chemical Structure, and Blend Behavior. *Macromolecules* **2004**, *37* (18), 6904−6911.
(38) Fang, W.; Yang, S.; Wang, X.-L.; Yuan, T.-Q.; Sun, R.-C. Manufacture and Application of Lignin-Based Carbon Fibers (Lcfs) and Lignin-Based Carbon Nanofibers (Lcnfs). *Green Chem.* **2017**, *19* (8), 1794−1827.
(39) Kubo, S.; Kadla, J. F. Hydrogen Bonding in Lignin: A Fourier Transform Infrared Model Compound Study. *Biomacromolecules* **2005**, *6* (5), 2815−2821.
(40) Ugartondo, V.; Mitjans, M.; Vinardell, M. P. Comparative Antioxidant and Cytotoxic Effects of Lignins from Different Sources. *Bioresour. Technol.* **2008**, *99* (14), 6683−6687.
(41) Núñez-Flores, R.; Giménez, B.; Fernández-Martín, F.; López-Caballero, M. E.; Montero, M. P.; Gómez-Guillén, M. C. Role of Lignosulphonate in Properties of Fish Gelatin Films. *Food Hydrocolloids* **2012**, *27* (1), 60−71.
(42) Barapatre, A.; Aadil, K. R.; Tiwary, B. N.; Jha, H. In Vitro Antioxidant and Antidiabetic Activities of Biomodified Lignin from Acacia Nilotica Wood. *Int. J. Biol. Macromol.* **2015**, *75*, 81−89.
(43) Santiago, J. A.; Pogemiller, R.; Ogle, B. M. Heterogeneous Differentiation of Human Mesenchymal Stem Cells in Response to Extended Culture in Extracellular Matrices. *Tissue Eng., Part A* **2009**, *15* (12), 3911−3922.
(44) Trivedi, P.; Hematti, P. Derivation and Immunological Characterization of Mesenchymal Stromal Cells from Human Embryonic Stem Cells. *Exp. Hematol.* **2008**, *36* (3), 350−359.
(45) Raub, C. B.; Putnam, A. J.; Tromberg, B. J.; George, S. C. Predicting Bulk Mechanical Properties of Cellularized Collagen Gels using Multiphoton Microscopy. *Acta Biomater.* **2010**, *6* (12), 4657−4665.
(46) Moraes, J.; Simionca, I.-M.; Ketari, H.; Klok, H.-A. Avoiding Compositional Drift During the RAFT Copolymerization of N-(2-Hydroxypropyl)Methacrylamide and N-Acryloxysuccinimide: Towards Uniform Platforms for Post-Polymerization Modification. *Polym. Chem.* **2015**, *6* (17), 3245−3251.
(47) Stavolone, L.; Lionetti, V. Extracellular Matrix in Plants and Animals: Hooks and Locks for Viruses. *Front. Microbiol.* **2017**, *8* (1760), 1.
(48) Yu, G.; Li, B.; Wang, H.; Liu, C.; Mu, X. Preparation of Concrete Superplasticizer by Oxidation-Sulfomethylation of Sodium Lignosulfonate. *BioResources* **2012**, *8* (1), 1055−1063.
(49) Koos, E.; Willenbacher, N. Capillary Forces in Suspension Rheology. *Science* **2011**, *331* (6019), 897−900.
(50) Kord Forooshani, P.; Lee, B. P. Recent Approaches in Designing Bioadhesive Materials Inspired by Mussel Adhesive Protein. *J. Polym. Sci., Part A: Polym. Chem.* **2017**, *55* (1), 9−33.
(51) Jung, J. P.; Sprangers, A. J.; Byce, J. R.; Su, J.; Squirrell, J. M.; Messersmith, P. B.; Eliceiri, K. W.; Ogle, B. M. ECM-Incorporated Hydrogels Cross-Linked via Native Chemical Ligation to Engineer Stem Cell Microenvironments. *Biomacromolecules* **2013**, *14* (9), 3102−3111.
(52) Jung, J. P.; Nagaraj, A. K.; Fox, E. K.; Rudra, J. S.; Devgun, J. M.; Collier, J. H. Co-Assembling Peptides as Defined Matrices for Endothelial Cells. *Biomaterials* **2009**, *30* (12), 2400−2410.
(53) Greene, T.; Lin, C.-C. Modular Cross-Linking of Gelatin-Based Thiol-Norbornene Hydrogels for in Vitro 3D Culture of Hepatocellular Carcinoma Cells. *ACS Biomater. Sci. Eng.* **2015**, *1* (12), 1314−1323.

DOI: 10.1021/acsabm.9b00444
ACS Appl. Bio Mater. 2019, 2, 3562−3572